BULLETIN OF THE POLISH ACADEMY OF SCIENCES
TECHNICAL SCIENCES, Vol. 58, No. 4, 2010
DOI: 10.2478/v10175-010-0045-z

GaAs/AlGaAs (∼9.4 μm) quantum cascade lasers operating at 260 K

M. BUGAJSKI*, K. KOSIEL, A. SZERLING, J. KUBACKA-TRACZYK, I. SANKOWSKA, P. KARBOWNIK, A. TRAJNEROWICZ, E. PRUSZYŃSKA KARBOWNIK, K. PIERŚCIŃSKI, and D. PIERŚCIŃSKA

Institute of Electron Technology, 32/46 Lotników Ave., 02-668 Warszawa, Poland

Abstract. The fabrication of Quantum Cascade Lasers (QCLs) emitting at ∼9.4 μm is reported. The devices operated in pulsed mode at up to 260 K. The peak powers recorded in 77 K were over 1 W, and the slope efficiency $\eta \approx 0.5$–0.6 W/A per uncoated facet. This has been achieved by the use of GaAs/$Al_{0.45}Ga_{0.55}As$ heterostructure, with 3QW anticrossed-diagonal design originally proposed by Page et al. [1]. Double plasmon planar confinement with Al-free waveguide has been used to minimize absorption losses. The double trench lasers were fabricated using standard processing technology, i.e., wet etching and Si_3N_4 for electrical insulation. The QCL structures have been grown by Molecular Beam Epitaxy (MBE), with Riber Compact 21T reactor. The stringent requirements – placed particularly on the epitaxial technology – and the influence of technological conditions on the device structure properties are presented and discussed in depth.

Key words: quantum cascade lasers, pulsed mode.

1. Introduction

The quantum cascade lasers (QCLs) are unipolar devices based on tunnelling and intersubband transitions, in which the electronic states, wave functions and lifetimes of relevant states are engineered through the quantum mechanical confinement imposed by a complex multilayer structure [2, 3]. The second main feature of this type of lasers is the cascading scheme of carriers route through the laser active region. That means the single carrier is used more than one time for generating photon – at best the number of generated photons is equal to the number of QCL modules, through which the carrier is cascaded. For QCLs to work, the extremely precise tailoring of energy levels of quantum states, optical dipole matrix elements, tunnelling times and scattering rates of carriers is required. The next critical issue for laser operation is the concentration of carriers in the structure.

Thus the principle of operation of QCL structures places stringent requirements on the individual layer thickness and composition as well as the overall periodicity of the whole structure. The laser operation is possible only when the designed structure is strictly realized, with the extreme technological precision concerning geometrical and doping features. For the mid-infrared (MIR) emitters the overall thickness tolerance seems to be only a few percent. On the basis of our experimental statistics we believe that the thickness tolerance limit is ∼3%. For the deviation from original design exceeding this value the devices will not lase. The similar, or even better accuracy, is required for the composition of layers. For emitters working at longer wavelengths (e.g., in the FIR region) the thickness tolerance is probably even sharper. That is why the technology of epitaxy used for QCL heterostructures must be characterized by long time stability of growth parameters as well as run-to-run reproducibility.

Another crucial problem of QCLs' operation are the heating effects, which are distinctly larger than in the state-of-the-art bipolar lasers. This is connected with the "natural" processes of depopulation of the lower laser level and carrier thermalization in the injector, by scattering with the optical or acoustic phonons. The heating results in the higher threshold and operation currents of the lasers, and all this in turn results in the necessity of the effective heat extraction. The heat dissipation in QCLs is strongly hampered because of the nature of their active regions containing many interfaces, and layers with thicknesses similar to the mean free path of phonons.

The physical basis of QCLs operation principle is fundamentally different from that of the "classical" bipolar semiconductor lasers, in which the emission is due to the interband radiative recombination of pairs of carriers instead of intersubband transitions which lead to lasing in QCLs. This fact influences the shape of gain as a function of quantum energy. Hence, the quantum cascade lasers with their narrow spectral gain, resemble the emitters which are based on electron transitions between energy levels in individual atoms, i.e., the gas lasers or solid-state lasers.

The available QCL emitter wavelength range at the moment spans from 3.5 μm up to 250 μm, so it generally covers the very wide infrared (IR) spectrum, from middle-IR (MIR) up to far-IR (FIR). In comparison with the performance of bipolar lasers, this is about two orders of magnitude increase of the wavelength range available for semiconductor lasers, towards the longer wavelengths, with the exclusion of the so called Reststrahlen region of radiation (i.e., 30–60 μm), where the photon energies match that of optical phonons which results in strong absorption by the semiconductor material. The huge spectral flexibility of the emission is a result of the used intraband generation mechanism.

*e-mail: bugajski@ite.waw.pl

QCLs may be used in free-space communication systems, molecular spectroscopy and imaging, for science, biomedicine, military purposes and public security. Their wavelength range covers the two optical windows (3–5 μm, 8–14 μm). On the other hand there is a variety of wavelengths absorbed by gases (e.g. by NO, CH_4, CO_2, CO etc.), in the range of 3.5–24 μm. The very wide spectral range as well as the possible wavelength control (obtained in distributed feedback lasers – DFBs) and wavelength tunability (for example by temperature or supply current changes) of QCLs are their great advantage.

The fast development in the field of QCLs is clearly observable, as for example the first continuous wave (CW) (operating at cryogenic temperatures) as well as the first room-temperature lasers have been demonstrated just a year after constructing the first QCL. Again, roughly one year periods separate the events of obtaining the first DFB-QCL laser, the first superlattice-QCL (SL-QCL), the first trace gas sensing made by use of DFB-QCL, the first mode-locked QCL, and the successful increasing of the lasing wavelength beyond 20 μm.

In this paper we present the development of mid-infrared GaAs/AlGaAs QCLs technology and discuss basic characteristics of lasers fabricated at the Department of Photonics at the Institute of Electron Technology.

2. MBE technology for the $Al_{0.45}Ga_{0.55}As$/GaAs QCLs

The active region of the laser structure studied in this paper (Fig. 1) was the 36 period sequence of modules made of $Al_{0.45}Ga_{0.55}As$/GaAs coupled quantum wells. The application of relatively high Al contents in AlGaAs layers, and hence the significant height of barriers improves the thermal performance of the devices [3], in comparison with the earlier AlGaAs/GaAs QCL construction [4]. Every module was composed of quasi-superlattice injector and emitting region based upon the three quantum level design (3QW). The electronic band structure of QCL has been calculated by solving Schroedinger equation with position dependent effective mass by finite difference method (FDM) [5] – see Fig. 2. The essential features of the considered design are diagonal anti-crossed transitions [4] from state E3 to E2 and depopulation of the laser ground state E2 by resonant optical phonon (LO^{Γ}) emission and tunnelling into the injector. The calculated lifetime of the excited state and dipole matrix element are $\tau_3 = 1.4$ ps, and $z_{32} = 1.71$ nm, respectively. The ground state E2 is depopulated in the time $\tau_{2-1} \sim 0.3$ ps [5]. These calculations were done at 48 kV/cm, close to estimated laser threshold.

The injector region, apart of its function connected with the relaxation and injection of electrons, plays also the role of a Bragg reflector preventing electrons from previous section, from escaping into the continuum. Only two central, barrier-QW pairs inside each injector have been doped. The investigated range of the injector doping was 0.4×10^{12}–2.2×10^{12} cm^{-2} per period. The doping is necessary to provide carriers, while preserving the overall charge neutrality of the device.

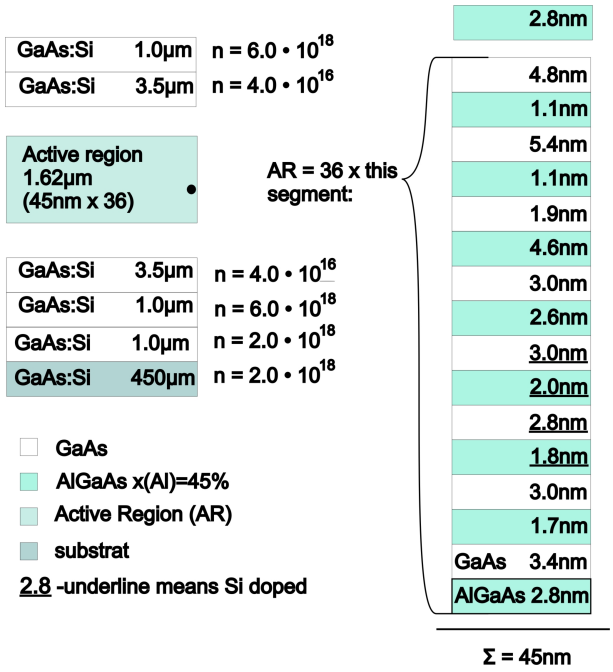

Fig. 1. Layer sequence in the $Al_{0.45}Ga_{0.55}As$/GaAs laser structure

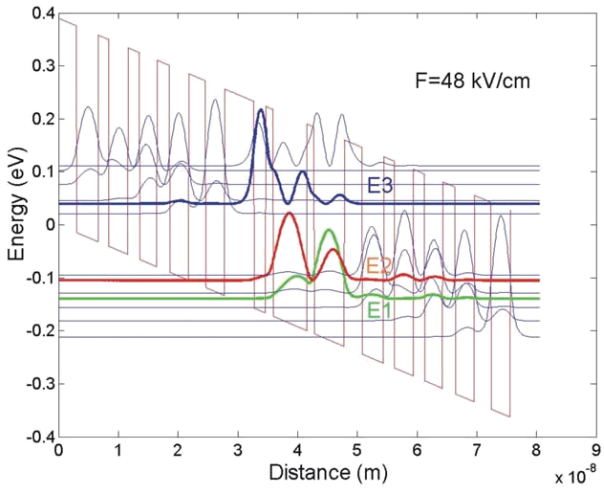

Fig. 2. Conduction band profile and moduli squared wavefunctions in injector/active/injector segment of the laser under the applied field of 48 kV/cm. The wavefunctions have been shifted to the energy positions of the respective levels. The E3, E2 and E1 refer to the upper, lower and ground state of lasing transitions. The thin blue lines are the injector lower miniband states. The lowest energy state in the injector couples directly to the upper laser level E3. The topmost state is the Γ continuum state. It is located ~80 meV above the upper laser level. The calculated energy differences $E_{32} = 147.1$ meV ($\lambda = 8.4$ μm) and $E_{21} = 38.5$ meV

The active region of the device was built into the double-plasmon Al-free waveguide, for planar optical confinement. The waveguide was made of the lightly doped GaAs (4×10^{16} cm^{-3}) enclosed with highly doped claddings (6×10^{18} cm^{-3}). Such a waveguide is much less lossy than

the one made of the AlGaAs/GaAs system, and based on the refractive index contrast of the involved materials. The main disadvantage of the AlGaAs/GaAs, results from the relatively low value of this contrast in the IR wavelength region of interest. The high radiation losses experienced in AlGaAs/GaAs waveguide are the result of radiation leakage beyond the AlGaAs cladding region and subsequent free-carrier absorption, as the cladding has to be doped. On the contrary, though the Al-free plasmon waveguide is enclosed by the highly doped GaAs cladding layers, they are not penetrated by the laser mode which means that when the waveguide is designed properly, it offers very efficient confinement of the IR radiation without excessive absorption losses. Essentially the waveguide design is a trade off between confinement and losses.

The laser structures were grown by solid source MBE in Riber Compact 21T reactor. The beams of the group III elements (6.5N Al and 7N Ga) were generated by using the standard ABN 80 DF effusion cells. The beam of As_4 molecules was produced by the valved-cracker As effusion cell. The (100) oriented GaAs n+ substrates were used. The substrate temperature T_s, controlled on the surface of the growing crystal by a pyrometer, was kept at 580°C. The value of V/III ratio was at least 35 for growth of both GaAs and $Al_{0.45}Ga_{0.55}As$ layers. Detailed analysis of the growth optimization procedures can be found in Ref. [6].

A very important for the technology development was the ability to predict theoretically the properties of the structures with varied design as well as the possibility to evaluate the influence of a particular design feature on the lasing ability of the devices. The above was provided by the theoretical model of the device electronic band structure. The appropriate software package has been developed in Matlab. It allows for calculating relevant properties of the structures depending on their geometry and applied electric field. These include: solving Schroedinger equation for energies and wavefunctions, as well as calculating dipole matrix elements, LO phonon scattering rates, lifetimes and transition rates. The software was tested by comparing results of calculations for structures published in the literature with reported data. The selected results were also compared with the ones obtained by using nextnano[3] package [7]. The developed software package was used for optimization of the QCL technology.

The High Resolution X-Ray Diffractometry (HRXRD) was the basic method for verifying the thicknesses and compositions of layers as well as periodicity of the cascade structure. The measurements have been performed by X'pert PRO PANalytical diffractometer. The X-Ray diffractometry has been used both for in depth study of QCL properties as well as for on-line examination of grown structures and has been found crucial for technology development.

The laser operation is possible only when the designed structure is strictly realized, with the extreme technological precision concerning geometrical and doping features. To calibrate growth rates of consisting binaries, an appropriate complex procedure has been developed. It has in particular employed the RHEED oscillations technique as well as X-ray diffraction (XRD) characterizations of test superlattice structures. For the analysis of double-crystal rocking curves (i.e., for simulating the symmetric (004) reflections) the dynamical diffraction theory has been used. Figure 3 presents the series of experimental diffraction curves for a number of consecutive growth runs compared to theoretical curve for intended structure.

Detailed analysis of measured HRXRD triple-axis $2\theta/\omega$ scans shown in Fig. 3 documents almost perfect agreement between optimized laser structure and simulated one referring to the intended design. This is seen from matching the measured and calculated satellite peak positions, as well as the positions of peaks corresponding with the mean composition of the heterostructure. About 1% thickness accuracy has been routinely achieved for lasing structures. The barrier layers have been found to contain (45±1)% of Al, which is, however, not that critical for lasing as the possible thickness inaccuracy. All the above mentioned features of diffraction curves, and particularly the numerous and narrow satellite peaks, document strict periodicity of the structures.

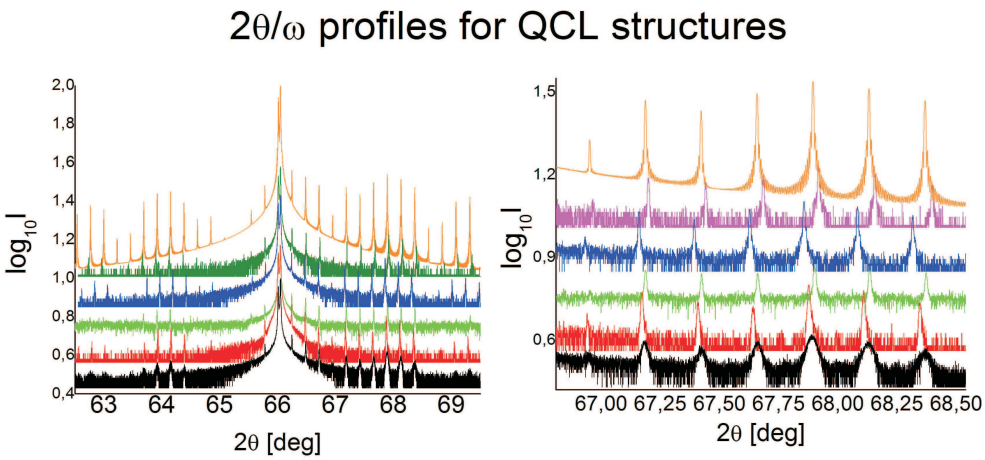

Fig. 3. HRXRD $2\theta/\omega$ curves for a series of QCL heterostructures grown in IET; the top curve is a simulation for the planned structure

3. Device processing and characterisation

The double trench lasers were fabricated using standard processing technology, i.e., wet etching and Si_3N_4 for electrical insulation. The low resistivity Ni/AuGe/Ni/Au ohmic contacts, alloyed in 430°C, were used at the top of the devices. For current injection, windows were opened through the insulator with width 25 and 35 μm. After the wafer was thinned down to about 100 μm, an alloyed AuGe/Ni/Au contact was deposited on the backside. The lasers were cleaved into bars of 0.5 mm, 1 mm and 2 mm length and soldered with Au/Sn eutectic, epilayer down on diamond heatspreader and copper submounts (Fig. 4). For some devices chips were soldered directly to heatspreader.

a)

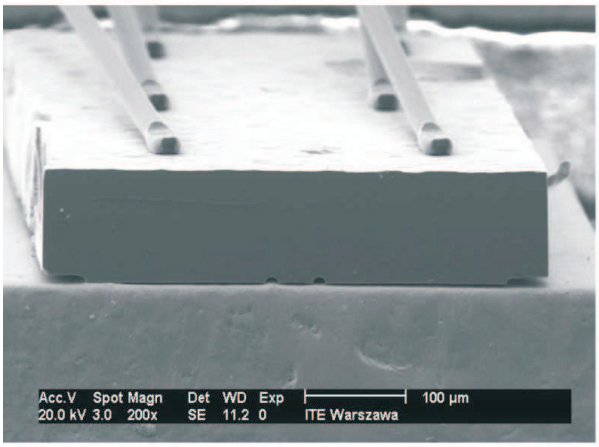

b)

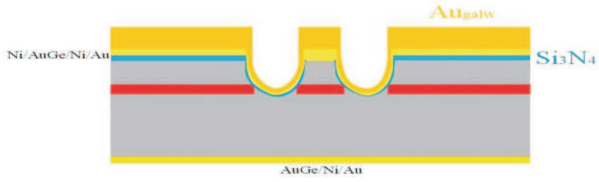

Fig. 4. a) SEM photograph of $Al_{0.45}Ga_{0.55}As$/GaAs quantum cascade laser soldered epi-down on diamond heatspreader and copper submount, b) cross-section of the device

The current-voltage characteristics, obtained for the structures in which the thickness and composition of active region layers were correctly engineered, are characterized by specific features (see Fig. 5). At low bias QCL structures should be highly resistive. When the electric field reaches the value for which the alignment of the upper laser state and the injector ground state takes place, electrons start flowing through the device. In this regime the operating voltage increases linearly with injection current. The saturation of the V-I characteristics, i.e., the high differential resistance of the device, is caused by the onset of misalignment between the upper laser level and the injector ground state. The above description should match the results of V-I measurements performed at low temperature (77 K); for higher temperatures the lower values of device differential resistance at all current regimes are observed are as a rule.

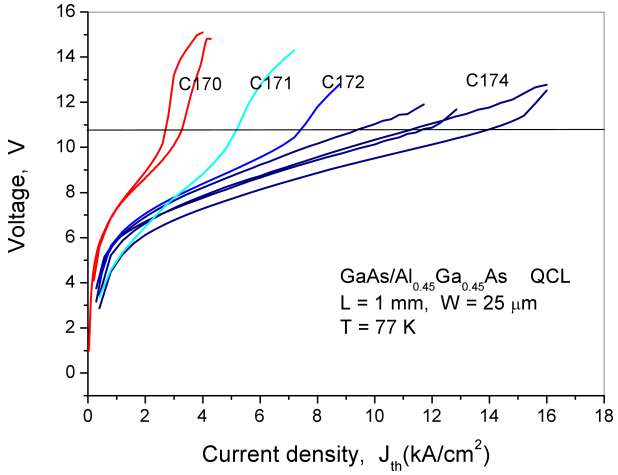

Fig. 5. Voltage-current characteristics for a set of $Al_{0.45}Ga_{0.55}As$/GaAs QCLs with different injector doping level ($\sim$0.4–$\sim$2.2$\times10^{12}$ cm^{-2} per period); the doping concentration increases from structure C170 to C174

The effect of saturation, limiting the dynamic range of laser operation depends on the injector doping concentration. As the threshold condition may be reached only after the gain exceeds the losses, it is possible that the saturation condition may appear before the losses are exceeded. That is why to achieve lasing the high enough currents must flow through the structure before the saturation, and this requirement has to be fulfilled by a proper injector doping. As the initially applied injector doping ($\sim0.4\times10^{12}$ cm^{-2}) was found to be too low to achieve lasing, the range of higher injector doping was tested for a fixed QCL geometrical construction. It occurred that much higher currents before the saturation were necessary for lasing, and hence the injector doping had to be increased substantially (at least to $\sim1.6\times10^{12}$ cm^{-2}).

Light output and current-voltage characteristics of the laser fabricated from GaAs/$Al_{0.45}Ga_{0.55}As$ heterostructure with different injector doping are shown in Fig. 6. The laser emission was recorded with TE cooled HgCdTe detector (type PVI-2TE-10- Vigo System S.A.). Light from the laser was shined directly on the detector (no collimating lens was used). The laser mirrors were uncoated and thus the output powers, for all (P-I) characteristics presented in this paper, refer to one mirror. For higher injector doping (2.2×10^{12} cm^{-2}) the average output power was 0.74 W and the average threshold current $J_{th} = 7.74$ kA/cm^{-2}, with the record power 1.14 W. The stimulated emission has been observed up to 1% filling factor, 8 μs pulse duration. The characteristic temperatures T_0 for the investigated lasers were typically of the order of 200 K and higher, which is value comparable with reported in literature. This value of T_0, should guarantee room temperature operation, providing that the 77 K threshold current density would be decreased to 3 kA/cm^{-2} range. The lowest threshold current density achieved so far in low doped structures equals to $J_{th} = 4.8$ kA/cm^{-2}. With $\sim$6 kA/cm^{-2} at 77 K extrapolated threshold current density at 300 K is $\sim$15 kA/cm^{-2} (see Fig. 7). Thus to avoid excessive heating it would be necessary to decrease ridge width below 20 μm.

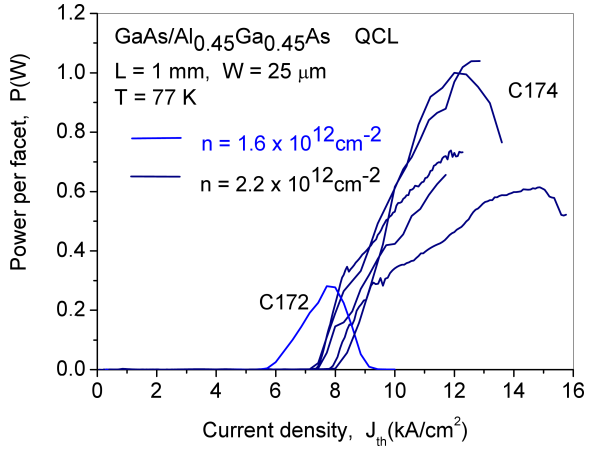

Fig. 6. Light-current (P-I) characteristics for lasers with different injector doping

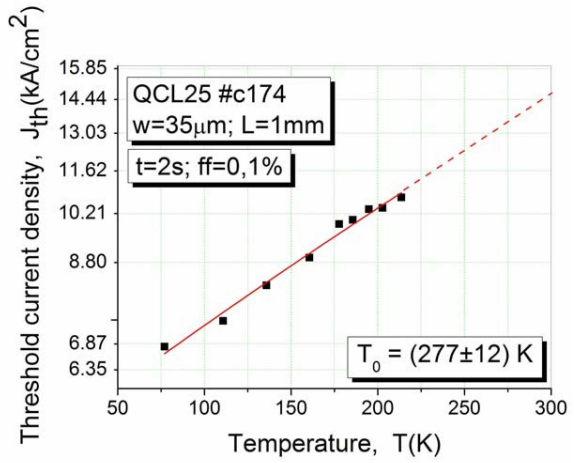

Fig. 7. Threshold current density as a function of temperature

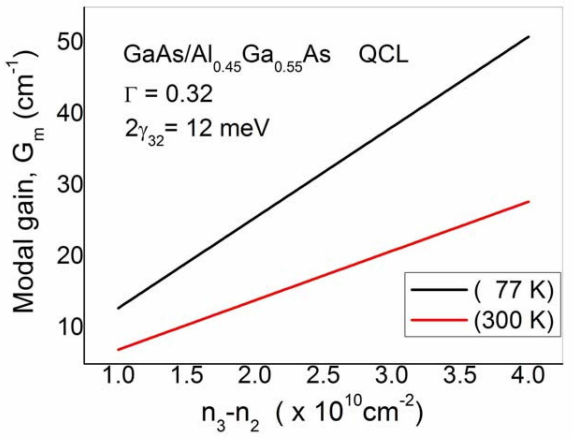

Fig. 8. Modal gain vs. inversion for different temperatures

The QCL threshold current density can be calculated from the equation [8]:

$$J_{th} = \frac{\varepsilon_0 n \lambda L_p \gamma_{32}}{4\pi e \Gamma |z_{32}|^2} \frac{\alpha_w + \alpha_m}{\tau_3(1 - \tau_{21}/\tau_{32})} \qquad (1)$$

where an injection efficiency of unity in the upper laser level E3 is assumed. In this equation, γ_{32} is the FWHM of the spontaneous emission spectrum and is directly related to the quality of interfaces. The meaning of the remaining parameters is as typically used. The analysis of the above equation with numerical values of parameters as given in [9] shows that to provide modal gain at least 20 cm^{-1} at room temperature we need inversion $\sim 3 \times 10^{10}$ cm^{-2} (Fig. 8), which should allow for threshold current densities in the range (3–4) kA/cm^{-2} at 77 K in good quality devices ($\gamma_{32} = (12 - 14)$ meV) – see Fig. 9.

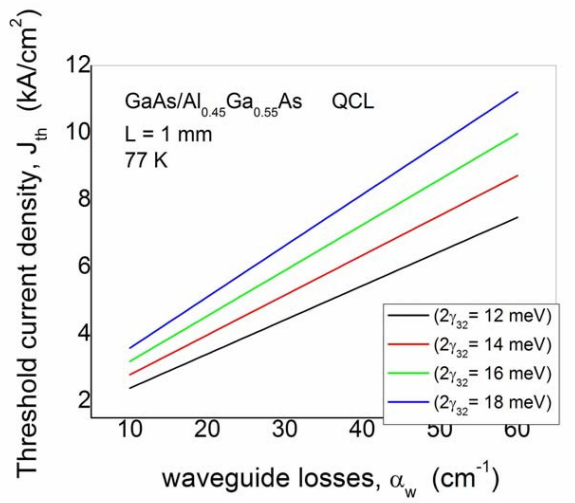

Fig. 9. Threshold current density vs. waveguide losses for different values of $2\gamma_{32}$ parameter

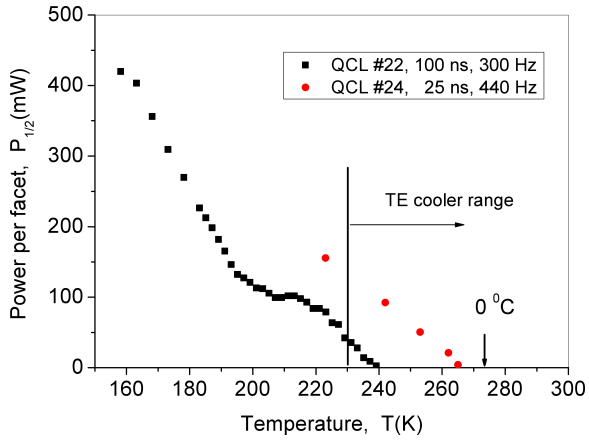

Fig. 10. Laser output versus temperature for two lasers operated at different pulse lengths

Laser output versus temperature for two lasers operated at different pulse lengths is shown in Fig. 10. It can be seen that the powers of 10–40 mW in the temperature range facilitated by two-stage TE Peltier coolers can be obtained, which means that developed lasers are suitable for outdoor applications as they operation is not limited by cryogenic cooling. There are also strong arguments that reaching true room temperature operation will be possible by improving device design; mainly by using narrower mesa and longer cavity.

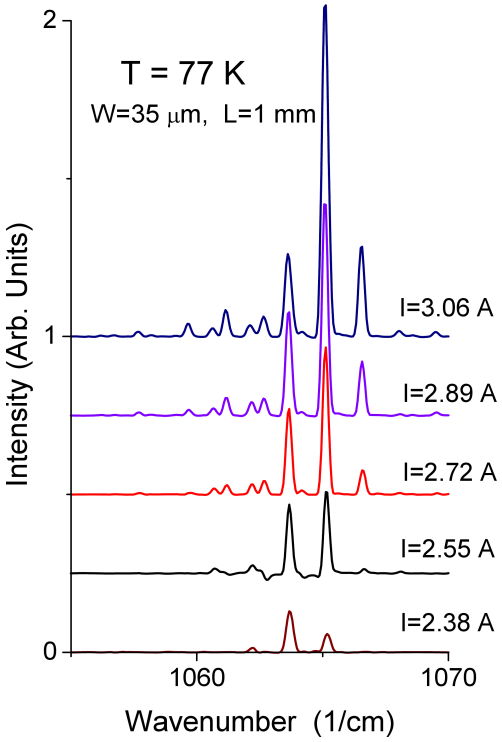

Fig. 11. QCL emission spectrum vs. supply current $I_{th} = 2.38$ A

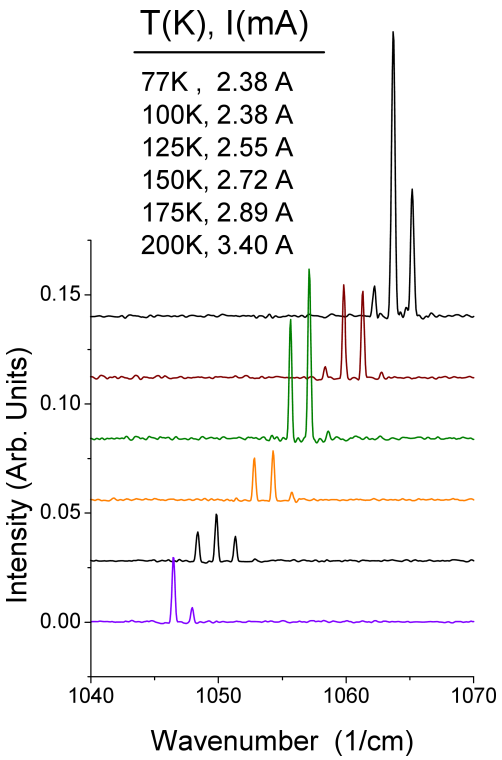

Fig. 12. QCL emission spectrum vs. temperature

The lasers emitted at ∼9.4 μm in a single transverse mode [10]. The spectrum consisted of a number of equally spaced longitudinal modes with mode spacing 1.47 cm^{-1} at 77 K and the full width at the half maximum of 0.26 cm^{-1} – see Fig. 11. With the increase of temperature the spectrum shifts towards the lower wavenumbers, with the speed of 0.17 cm^{-1}/K – see Fig. 12.

4. Conclusions

The development of (λ ∼9.4 μm) GaAs-based quantum cascade lasers (QCLs) operating up to 260K is reported. This has been achieved by the use of GaAs/$Al_{0.45}Ga_{0.55}As$ heterostructures. The laser design followed an 3QW anticrossed-diagonal scheme. The QCL structures were grown by MBE, with Riber Compact 21T reactor. The peak powers recorded in 77 K were over 1 W, and the slope efficiency η ≈0.5–0.6 W/A per uncoated facet. These results are fully comparable with the state of the art devices of similar design produced in other laboratories. The developed lasers are suitable for outdoor applications.

Acknowledgements. The work was financially supported by the Grant PBZ-MIN-02/I/2007.

REFERENCES

[1] H. Page, C. Becker, A. Robertson, G. Glastre, V. Ortiz, and C. Sirtori, "300 K operation of GaAs based quantum-cascade laser at $\lambda \approx 9$ μm", *Appl. Phys. Lett.* 78, 3529–3531 (2001).

[2] C. Sirtori, "*GaAs* quantum cascade lasers: fundamentals and performance", *EDP Sciences* 7, 1–20 (2002).

[3] C. Gmachl, F. Capasso, D.L. Sivco, and A.Y. Cho, "Recent progress in quantum cascade lasers and applications", *Rep. Prog. Phys.* 64, 1533–1601 (2001).

[4] C. Sirtori, P. Kruck, S. Barbieri, P. Collot, J. Nagle, M. Beck, J. Faist, and U. Oesterle, "GaAs/AlGaAs quantum cascade lasers", *Appl. Phys. Lett.* 73, 3486–3488 (1998).

[5] P. Harrison, *Quantum Wells, Wires and Dots: Theoretical and Computational Physics*, Willey, Chichester, 2005.

[6] K. Kosiel, J. Kubacka-Traczyk, P. Karbownik, A. Szerling, J. Muszalski, M. Bugajski, P. Romanowski, J.Gaca, and M. Wójcik, "Molecular beam epitaxy growth and characterization of mid-infrared quantum cascade laser structures", *Microelectronics J.* 40, 565–569 (2008).

[7] http://www.nextnano.de, 2009.

[8] K. Kosiel, M. Bugajski, A. Szerling, J. Kubacka-Traczyk, P. Karbownik, E. Pruszyńska-Karbownik, J. Muszalski, A. Łaszcz, P. Romanowski, M. Wasiak, W. Nakwaski, I. Makarowa, and P. Perlin, "77 K operation of AlGaAs/GaAs quantum cascade laser at 9 μm", *Photonics Letters of Poland* 1, 16–18 (2009).

[9] S. Hofling, V. D. Jovanovic, D. Indjin, J.P. Reithmaier, A. Forchel, Z. Ikonic, N. Vukmirovic, and P. Harrison, "Dependence of saturation effects on electron confinement and injector doping in GaAs/$Al_{0.45}Ga_{0.55}As$ quantum-cascade lasers", *Appl. Phys. Lett.* 88, 251109–251111 (2006).

[10] A. Szerling, P. Karbownik, E. Pruszyńska-Karbownik, K. Kosiel, M. Bugajski, S.Adhi, T. Ochalski, and G. Huyet, "Electrical and optical characterisation of (λ ∼9.4 μm) GaAs-based quantum cascade lasers", *IEEE Proc. TERA-MIR* 1, 71–72 (2009).